Ultrafast Rotational Anisotropy Measurements: Strong-Field Nonlinear Saturation Effects

Emily J. Brown, Igor Pastirk,† and Marcos Dantus*

Department of Chemistry and Center for Fundamental Materials Research, Michigan State University, East Lansing, Michigan 48824

Received: February 12, 2001; In Final Form: June 17, 2001

Nonlinear saturation effects in ultrafast time-resolved rotational anisotropy measurements are explored as a function of increased pump laser intensity. Femtosecond pump−probe experimental data were obtained over 3 orders of magnitude in pump laser intensity ranging from no saturation to highly nonlinear saturation. Data were obtained for molecular iodine vapor at room temperature following resonant excitation of the B←X transition. For low pump laser intensities, the data are shown to fit the conventional anisotropy formalism for unidirectional detection well. For higher pump laser intensities, the overall anisotropy diminishes because of saturation and the conventional fits diverge from the experimental data. In this regime, a saturation parameter can be introduced in the formulation to improve the fit between the model and the experimental data, thereby improving the accuracy of the resulting rotational temperatures. At the highest laser intensities, an additional photochemical pathway arising from the A←X transition is observed. Incorporation of this pathway into the nonlinear rotational anisotropy model yields accurate rotational populations even for the highest laser intensities. Applications of this nonlinear anisotropy model to reactive and nonreactive ultrafast studies in order to extract quantitative information are discussed.

I. Introduction

Ultrafast pump−probe spectroscopy has proven to be extremely useful in elucidating the molecular dynamics of nonreactive and reactive systems.[1−3] Observations of vibrational and rotational motion in gas-phase samples yield information regarding bond formation and bond breakage (which can lead to determining reaction mechanisms) as well as information about the molecular structure and rotational populations of the species involved. For example, see Refs 4−7.

Classical and quantum mechanical descriptions of rotational anisotropy measurements are well-known.[4,8−10] As discussed in recent papers from our group,[5,6,11−14] it is sometimes necessary to adapt these well-known equations in order to extract accurate rotational constants and/or rotational populations based on the experimental methods (e.g., pump−probe,[12] transient grating,[11,13] four-wave mixing,[14] and multiphoton ionization[5,6]). The anisotropy formulas were originally derived assuming weak-field interactions.[15] Because the peak intensities of femtosecond laser pulses can typically approach 10^{12} W/cm^2 levels, it is important to consider the role of saturation and other field-induced effects on anisotropy measurements and how these nonlinear phenomena must be included in the analysis to extract accurate information. In the case of severe saturation, other photophysical and photochemical pathways become available. These may include multiphoton excitation, ionization, and dissociation.

From a theoretical standpoint, the rotational anisotropy at time zero and time infinity are well-defined for a given experiment.[4,12] We have observed that as the intensity of the pump laser increases, the time-resolved measurements no longer reflect an accurate rotational distribution. This shortcoming implies that quantitative information derived from ultrafast rotational anisotropy (URA) measurements may not truthfully reflect the rotational populations and dynamics of the system when the laser intensity is high.

In this paper, we explore saturation effects as well as the possibility of additional excited state interactions as a function of pump laser intensity. Experimental URA data are presented for gas-phase iodine using a pump laser that is adjusted over 3 orders of magnitude in intensity and a weak probe pulse where the intensity is not adjusted. Here, the anisotropy formulation[12] is modified to accommodate saturation and additional photochemical channels that influence the URA measurements following strong-field excitation. Implications of these measurements to the characterization of rotational dynamics, distributions, and temperatures are discussed.

II. Theory

A. Strong-fields and Molecular Alignment. The observation of molecular alignment stemming from high intensity nonresonant laser excitation has been theoretically explored by Friedrich and Hershbach.[16,17] In the laser-induced alignment method, the intense laser field causes an induced dipole in polarizable molecules, which suppresses the rotational motion and leads to aligned pendular states.[16,17] Friedrich and Herschbach developed this laser-induced alignment theory based on earlier observations of dissociative multiphoton ionization experiments on CO and I_2 with intense infrared lasers conducted by Normand et al.[18] and Dietrich et al.,[19] respectively. In these cases, either the parent molecule was forced to align along the polarization vector of the laser before dissociation[18] or a torque was imparted on the molecule thereby causing a gain of angular momentum.[19] Demonstrations of the laser-induced alignment technique have been conducted by Kim and Felker on large nonpolar molecules[20,21] and by Stapelfeldt and co-workers on smaller

* To whom correspondence should be addressed. E-mail: dantus@cem.msu.edu.

† Affiliated with the Institute for Nuclear Sciences "VINCA", Belgrade, F. R. Yugoslavia.

10.1021/jp010543a CCC: $20.00
Published on Web 07/31/2001

nonpolar molecules.[22,23] Posthumus et al. have examined the multiphoton dissociative ionization of H_2, N_2, and I_2 with 50 fs pulses and found that only H_2 and N_2 showed alignment characteristics.[24] Corkum and co-workers have combined intense off-resonance chirped circularly polarized fields to induce rotational acceleration, thus constructing a molecular centrifuge.[25] Fujimura's group is currently exploring the deformation of molecules in the presence of strong-fields.[26] Experimental findings from our group indicate that CS_2 molecules bend in the presence of strong off-resonance fields. Those experiments were carried out by measuring the field-free rotational recurrence observed ~76 ps after strong-field excitation in a transient grating experiment.[13,27]

Alignment with resonant intense laser fields has been examined theoretically by Tamar Seideman. When on-resonance fields are used, the intensity does not have to be as strong as in off-resonance experiments to generate alignment.[28] She noted that for heavier molecules (which would correspond to greater rotational periods), a longer laser pulse duration is required to align the molecules; in addition, she also noted that nonresonant experiments may be more advantageous for these larger molecules under low initial rotational temperature conditions.[28] Finally, in these experiments, the alignment survives and recurs at specific times after the field is turned off. Similarly, Ortigoso et al. have calculated the conditions (laser pulse and rotational constant of the molecule) for which recurrences of the laser-induced alignment can be expected with nonresonant short pulses.[29]

The experimental work presented here involves moderately intense femtosecond laser pulses that are resonant with the electronic transitions of I_2. On the basis of the results and conclusions of the above on- and off-resonance studies, adiabatic alignment is not expected because of the short duration of the laser pulses, the mass of the iodine molecule, and the warm initial rotational temperature of the molecules (294 K). The goal of this work is to explore how nonlinear processes brought about by resonant fields influence rotational anisotropy measurements.

B. Rotational Anisotropy Measurements. Molecular iodine was chosen as a model system for these measurements based on the fact that it is one of the best studied molecules by time-resolved methods.[30−37] The experiments measure the initial alignment and subsequent rotational dephasing of iodine molecules that absorb a photon in a parallel transition from the ground X ($^1\Sigma_{0+g}$) state[38] to the excited B ($^3\Pi_{0+u}$) state.[39] The probe laser excites molecules in the B state to the E (0^+_g) and f (0^+_g) ion pair states.[40−43] The signal for the measurements presented here is the laser induced fluorescence (LIF) from the f ion pair state to the B state at 340 nm[42,43] unless otherwise noted. The potential energy curves for these states are shown in Figure 1a. As will be discussed later, the A ($^3\Pi_{1u}$) and β (1_g) states are also accessible with the pump and probe lasers and are also shown in Figure 1a.

The time evolution of the rotational alignment is measured with linearly polarized lasers. Excitation by the pump pulse selects an initial population distribution described by $\cos^2\theta$ where θ is the angle between the transition dipole and the pump laser polarization vector.[44] (See Figure 1b.) As the distribution dephases due to rotations of the molecules, the probe pulse (polarized either parallel or perpendicular to the excitation pulse) is unable to excite all the molecules to another state, resulting in a decrease in the fluorescence from that state. This fluorescence is monitored as a function of time delay between pump and probe pulses. The time-resolved data for each polarization arrangement ($I_{||}$ and $I_\perp$, where || (parallel) and $\perp$ (perpendicular)

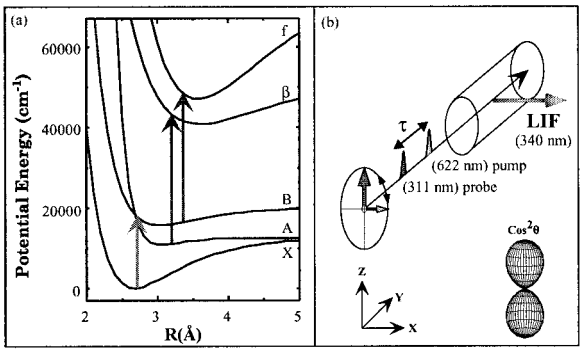

Figure 1. (a) Relevant potential energy curves for I_2. Molecules in the X state can be excited to the B state (parallel transition) and the A state (perpendicular transition) with 622 nm laser pulses. Excitation with 311 nm probe pulses will induce a transition between the B and f states (favored by parallel pump−probe beams) and between the A and β states (favored by perpendicular pump−probe beams). In both cases, LIF (f → B, β → A) at 340 nm is detected. (b) Experimental setup for rotational anisotropy measurements with unidirectional (*X*-axis) detection. The polarization of the probe beam remains oriented along the *Z*-axis, whereas the orientation of the polarization of the pump beam can be rotated along either the *X*- ($\perp$) or *Z*-axis (||). LIF is collected perpendicular to the propagation of the laser beams.

refer to the relative orientation of the polarization vectors of the pump and probe pulses) contain an isotropic component, reflecting molecular vibrations in this case, and an anisotropic component, reflecting rotational dephasing.

Semiclassically, the rotational anisotropy, $r(t)$, can be written as a weighted sum of the individual rotational state anisotropies, $r(j,t)$,[4,10]

$$r(t) = \frac{\sum_j P(j) r(j,t)}{\sum_j P(j)} \tag{1}$$

where $P(j)$ is the product state distribution, for example a Boltzmann or Gaussian distribution. The equations defining $r(t)$ are adapted to the specific experimental method used for the measurements.[4,6,12,13] In this experiment, the pump and probe excitations are one-photon transitions and we detect probe laser induced fluorescence (LIF) in one direction, specifically the *X*-direction (see Figure 1b). When the fluorescence is detected along the *X*-axis only, with $f \geq 3$ collection optics, the rotational anisotropy is obtained by

$$r(t)_X = \frac{I_{||} - I_\perp}{I_{||} + \frac{5}{2} I_\perp}, \tag{2}$$

as discussed in our previous paper.[12] We will use this equation to measure the rotational anisotropy from our experimental data here.

C. Effects of Saturation. The goal is to explore how the intensity of the pump laser affects URA measurements because of saturation in the B←X transition. The initial population impulsively excited by the pump pulse has a $\cos^2\theta$ distribution. (See Figure 1b.) As the intensity of the pump pulse increases, the population in the B state increases and the probability for stimulated emission increases as well. Hence, saturation occurs. Those molecules that are well aligned with the laser will be more susceptible to stimulated emission. Molecules with a smaller θ are more likely to experience saturation than those

with a larger θ. Therefore, the $\cos^2\theta$ distribution broadens. The end result is a reduction in the overall anisotropy. For these cases, we propose a modification of the state-resolved anisotropy equation (in the X-direction)[12] by including a saturation factor, A_S, to obtain

$$r_{AS}(j,t) = (1 - A_S)r_0(j,t) = (1 - A_S)\frac{2}{15}(1 + 2\cos(2\omega t)) \quad (3)$$

where $r_0(j,t)$ is the unperturbed rotational anisotropy, $\omega = 4\pi Bjc$, B is the rotational constant of the molecule, and c is the speed of light. The saturation parameter can vary between 0 and 1 (no saturation to severe saturation, respectively). As the pump laser intensity increases, A_S increases to take into account the reduction in the overall anisotropy.

Here, we present URA measurements that range over 3 orders of magnitude in laser intensity, from no saturation to highly nonlinear saturation of the B←X transition. We develop a correction to the model based on saturation and other nonlinear effects and demonstrate that all data become quantitatively correct. Our treatment concerns the first picoseconds of the URA measurements; however, they are applicable to all time domains where rotational quantum recurrences or revivals are observed.

III. Experimental Section

The experimental setup has been described elsewhere.[12,45] Experiments were carried out by 622 nm pump excitation of I_2 to the B state followed by probing at 311 nm which causes an excitation to the f state from which LIF was collected at 340 nm. For the f←B←X excitation pathway, the pump and probe excitations are one-photon parallel transitions and the unpolarized LIF was collected perpendicular to the propagation of the lasers. The signal collection was restricted to $f = 3$. The polarization of the 311 nm probe pulse was fixed (Z-axis in Figure 1b), whereas that of the 622 nm pump pulse was changed to be parallel or perpendicular relative to the probe pulse (Z- or X-axis in Figure 1 respectively) by a zeroth-order half-wavelength plate.

The polarization ratios (vertical:horizontal) of the pump and probe lasers were measured to ensure they were well polarized as in Ref 12; the pump laser polarization ratio was enhanced with a calcite polarizer placed after the half-wavelength plate. After the dichroic beam splitter that recombined the two beams, the probe laser polarization ratio was greater than 10^2:1 and the pump laser polarization ratio was greater than 10^4:1. These polarization ratios were also checked after the experimental cell; the polarization of the beams was maintained by the cell windows. The experimental transients were obtained by measuring the LIF as the time delay between the pump and probe pulses was varied. Parallel transients were obtained with the laser polarization vectors parallel; perpendicular transients were obtained when the laser polarization vectors were perpendicular. The parallel and perpendicular transients were examined to make sure that the time zero did not change when the polarization of the pump beam was rotated.

Neutral density filters were used to attenuate the pump laser intensity. In some cases, (0.056×10^{12} W/cm^2 and 0.27×10^{12} W/cm^2), the pulse width of the laser pulse was increased from 50 to 120 fs. This broadening reduced the peak intensity, thereby reducing nonlinear effects even further. Within each transient, the probe beam laser intensity (312 nm) was continuously measured by a photodiode and pulses with energy more than one standard deviation from the mean were discarded. A quartz cell containing iodine was prepared on a vacuum line and degassed to less than 10^{-6} Torr. The vapor pressure of I_2 is 0.25 Torr at the laboratory room temperature ($T_{RT} = 294 \pm 3$ K). URA measurements are not typically meant to provide highly accurate temperatures; they are usually used to determine the temperature of products from chemical reactions within a 10% margin of error. Here we show that this wide margin cannot be achieved if saturation occurs.

TABLE 1: Rotational temperatures (T_{fit}) resulting from the fits based on eq 3 (A) without the saturation parameter and (B) with the saturation parameter at different pump laser intensities[a]

intensity (10^{12}W/cm^2)	A. no saturation parameter (A_s=1.0) T_{fit} (K)		% error	B. saturation parameter A_S	T_{fit} (K)		% error
0.056	302	±22	2.7%				
0.27	290	±12	(1.4%)				
1.4	379	±23	29%	0.23	325	±22	11%
8.5	325	±22	11%	0.36	243	±15	(17%)
19	433	±34	47%	0.46	276	±17	(6.1%)
37	446	±47	52%	0.59	243	±22	(17%)
62	464	±55	58%	0.65	228	±30	(22%)

[a] Note that parentheses around a percentage indicate that the calculated temperature is below the actual temperature.

IV. Results and Discussion

One of the goals of this study was to determine how the accuracy in determining rotational distributions or rotational temperatures is compromised by saturation and other strong-field effects. To this end, all the laser intensity dependence measurements were carried out at room temperature, T_{RT}. The rotational temperature obtained from fitting each URA measurement, T_{fit}, was compared with T_{RT}. Each fit was found by calculating the experimental rotational anisotropy from the experimental transients using Equation 2, conducting a linear squares regression on the experimental $r(t)$, fitting it to Equation 1 where $r(j,t)$ is defined in Equation 3, and allowing the temperature, T_{fit}, to vary. The background and the saturation parameter, A_S, were also optimized to obtain the best fit to the experimental data. The agreement between T_{fit} and T_{RT} was used to evaluate the quality of the model.

A. Ultrafast Rotational Anisotropy: Weak-field Model. Parallel and perpendicular transients were measured over a range of pump laser intensities from 0.056×10^{12} W/cm^2 to 62×10^{12} W/cm^2. The URA measurement corresponding to each intensity was fit as described above, keeping the saturation factor at zero and varying only the temperature and background. As can be seen in Table 1A, at the two lowest laser intensities, the agreement with theory is very good with 1.4 to 2.7% deviation between T_{fit} and T_{RT}. However, the URA measurements obtained with higher pump laser intensities do not fit the conventional theory (up to 58% deviation) because of saturation effects.

The experimental URA data (squares) from the two lowest laser intensities are shown in Figure 2 along with the rotational temperature fits (lines). The time-resolved transients, $I_{||}$ and $I_{\perp}$, have been normalized such that the intensity at negative pump−probe time delays is 0 and the intensity at 6 ps (approaching time infinity) equals 2 for parallel transients and 1.3 for perpendicular transients before calculating $r(t)$ using Equation 2. (These values are obtained by examining the theoretical equations for $I_{||}$ and $I_{\perp}$ as the time delay approaches infinity. See Ref 12 for the relevant equations for unidirectional detection.) We observed that using normalized versus unnormalized data only changed the results slightly (± 3% for the rotational temperature). The data at these lower intensities reproduce the theoretical values for $r(0)$ and $r(\infty)$ with great

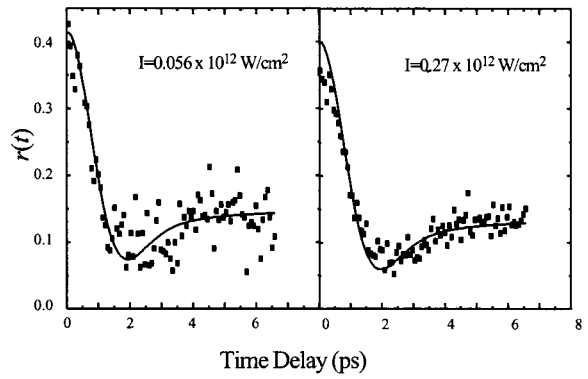

Figure 2. Rotational anisotropy of I_2 in the low pump laser intensity regime. Experimental data are shown by the square data points and the temperature fits are shown with the lines. These URA measurements are fit without the saturation parameter and accurately reflect the shape of the data.

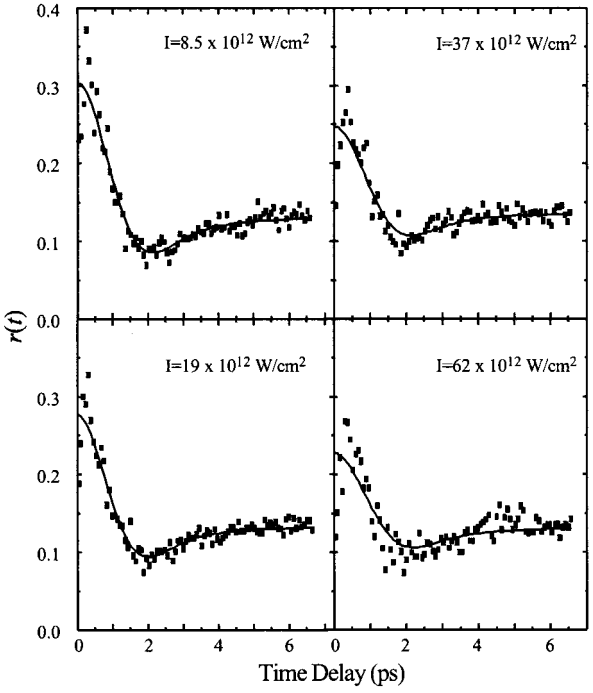

Figure 3. Rotational anisotropy of I_2 in the high pump laser intensity regime. These URA measurements are fit with the saturation parameter, A_S. This simple saturation model does not predict the observed dip in the data near time zero and yields rotational temperatures with 6−22% error.

accuracy. The higher intensity URA measurement (0.27×10^{12} W/cm^2) does show a slight decrease from the theoretical $r(0)$ value of 0.4 as saturation begins to play a role in the excitation process. The fits reflect thermal populations of 302 ± 22 K (0.056×10^{12} W/cm^2) 0.4and 290 ± 12 K (0.27×10^{12} W/cm^2) which agree with the laboratory temperature of 294 ± 3 K. The deviation observed in the weaker intensity transient is probably caused by the much lower signal-to-noise ratio of the data.

B. Ultrafast Rotational Anisotropy: Saturation Effects. The experimental URA data (squares) for strong-field excitation are shown in Figure 3. Notice the overall reduction in anisotropy and the appearance of a dip around time zero, $t < 500$ fs. In these cases, the saturation parameter, A_S, in addition to T_{fit} and the background were allowed to vary in the fitting procedure as described above. The results from these fits are shown in Table 1B. The fits give temperatures that do not correspond to T_{RT} (6.1−22% deviation) but are more accurate than the temperatures obtained without the saturation parameter (see above). From Figure 3, it is evident that the rotational temperature fits (lines) do not model the early time behavior properly because of the appearance of a dip in the experimental URA measurement. In addition, the fit at the bottom of the rotational anisotropy curve (near $t = 2$ ps) does not appear to model the data very well. The depletion feature near time zero cannot be addressed by the simple saturation model, leading to improper fits and resulting in inaccurate rotational temperatures. Therefore, a different process is responsible for these changes in the anisotropy for which the simple saturation model cannot account.

C. Ultrafast Rotational Anisotropy: Saturation and Reactive Pathway. In the case of iodine, high pump laser intensities allow not only stimulated emission but also the possibility of other pathways, e.g., multiphoton excitation, access to other states, etc. At the excitation wavelength of 622 nm, the repulsive wall of the A ($^3\Pi_{1u}$) state is accessible through the A ← X perpendicular transition.[46,47] The short-lived wave packet on the A state can be excited to the β (1_g) state by the 311 nm probe laser; this is a parallel transition. Interestingly, the $\beta \rightarrow$ A fluorescence coincides with the f → B transition at 340 nm.[48−50] Refer to Figure 1a for the relevant potential energy surfaces. At high intensities, the B state saturates; however, the A state, being reached at a steeply repulsive region, has a short-lived transition state and is not easily saturated. Therefore, as the B state becomes saturated at higher intensities, the weaker A state transition begins to play an important role in the excitation process. On the basis of the characteristics of the transitions (parallel or perpendicular), with parallel pump−probe beams, the B state is primarily observed; with perpendicular pump−probe beams, the A state is probed preferentially. The short-lived signal, arising from the perpendicular pump−probe arrangement, explains the dip in the URA observed near $t = 0$ fs at higher intensities (vide infra).

We have observed in our measured data ($I_{||}$ and $I_\perp$) that the first vibrational oscillation (nearest to $t = 0$) in the $I_\perp$ transients is more intense than the oscillations that follow it, particularly for the highest pump laser intensities. The $I_{||}$ transients do not exhibit a similar significant increase in the intensity of the first vibrational oscillation as compared to the subsequent ones. This effect can be predicted based on the extinction coefficients of the A−X (23.9 L mol^{-1} cm^{-1}) and the B−X (51 L mol^{-1} cm^{-1}) transitions[47] and the short lifetime of the wave packet excited above the dissociation energy of the A state. The Einstein coefficients are similar for the two spontaneous emission processes following the probe pulse: f → B at 341 nm is 712×10^5 s^{-1} and $\beta \rightarrow$ A at 341 nm is 745×10^5 s^{-1}.[50] These values allow us to calculate a parameter that depends on the ratio of the probability for probing these two pathways (β←A←X versus f←B←X), $A_{A/B} = 9$. At high intensities, $I_{||}$ decreases from saturation, whereas $I_\perp$ increases from the contribution from the A state that is preferentially probed in the perpendicular configuration near $t = 0$. Therefore, the expression ($I_{||} - I_\perp$) in the numerator of eq 2 becomes much smaller and $r(t)$ decreases. This effect can only be observed at short time delays because molecules reaching the A state dissociate in 200−300 fs (as measured by Zewail and coworkers who studied I_2 in solvent cages).[51,52] Therefore, the additional signal (a fast decaying, almost delta function) at $t = 0$ for perpendicular transients causes the dip in the URA measurements. This dip becomes larger with higher pump intensities and can be predicted by examining the intensity of the first oscillation in the perpendicular transients as a function of pump laser intensity.

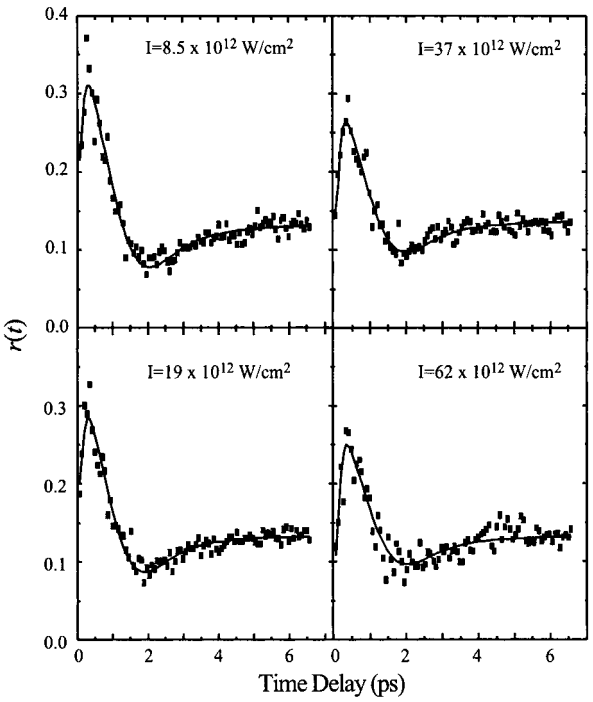

Figure 4. Rotational anisotropy of I_2 in the high pump laser intensity regime. The fits for these URA measurements include both the saturation effect, A_S, and reactive state interaction, $A_\perp$. The early time behavior is reflected well in this model. The rotational temperatures for the data at the four laser intensities shown are within 3.7−8.5% of the laboratory temperature.

To account for the additional state interaction, we propose the following model for the state-resolved rotational anisotropy

$$r_{A_S,\perp}(j,t) = (1 - A_S)r_0(j,t) - A_\perp e^{-(t/\tau)2} \qquad (4)$$

where the first term describes the reduction in the overall anisotropy caused by saturation of the B−X transition as in Equation 3 and the second term describes the dip at early times caused by the interaction of the repulsive A perpendicular state. $A_\perp$ accounts for the population in the A state and the Gaussian function accounts for the Gaussian spectral window of the probe and the temporal convolution of the laser pulses.

The experimental URA data (squares) obtained with high pump laser intensities are shown in Figure 4. In this case, the fits were obtained using Equation 1, where $r(j,t)$ is defined by Equation 4, and allowing A_S, $A_\perp$, T_{fit}, and the background to vary. In Equation 4, τ was set equal to 180 fs which corresponds to the fast dissociation convoluted with the cross correlation of our laser system for these measurements. The fits (lines) yield thermal populations that accurately reflect the laboratory temperature for all URA measurements at higher laser intensities (3.7−8.5% deviation for the strongest intensities; 14% for a moderate intensity, where eq 3 yielded more accurate results). See Table 2 for the temperatures obtained with the fits. The dip and subsequent rise near time zero in the data for each intensity is modeled well and the entire fit of the curve reflects the data more accurately as compared to the fits that do not include $A_\perp$ (compare Figures 3 and 4).

The trends in T_{fit} obtained with the three models are displayed in Figure 5; the broad gray line is T_{RT} (294 ± 3 K). As has been noted above, the no saturation model (dark gray squares) yields T_{fit} values that are much higher than the T_{RT} for the most intense fields. The simple saturation model (triangles) leads to temperatures closer to the laboratory temperature but are too low at the highest intensities. The model which incorporates both the saturation of the B−X transition and the reactive path from the A−X transition (black circles) results in temperatures closest to the actual temperature.

TABLE 2: Rotational Temperature Fits (T_{fit}) at Different Pump Laser Intensities Using eq 4 Which Includes Both the Saturation Parameter (A_S) and the Reactive Path Parameter ($A_\perp$)[a]

intensity (10^{12}W/cm^2)	saturation + perpendicular parameter				
	A_S	$A_\perp$	T_{fit} (K)		% error
1.4	0.18	0.042	336	±23	14%
8.5	0.24	0.14	269	±11	(8.5%)
19	0.34	0.12	309	±12	5.1%
37	0.45	0.15	283	±13	(3.7%)
62	0.49	0.17	273	±18	(7.1%)

[a] Parentheses around a percentage indicate that the calculated temperature is below the actual temperature.

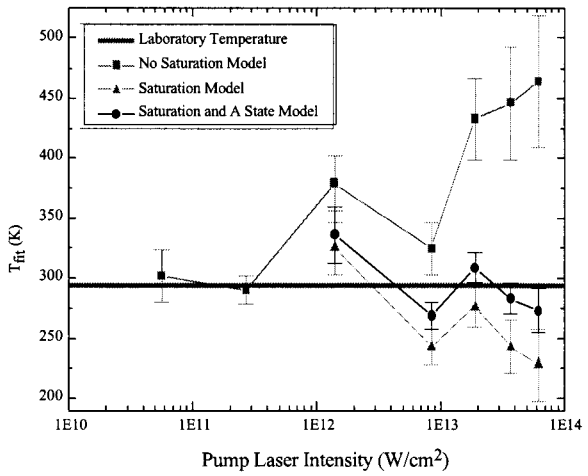

Figure 5. Rotational temperatures, T_{fit}, obtained from the three models used to fit the experimental rotational anisotropy data. The laboratory temperature, T_{RT} = 294 ± 3 K is shown as the broad gray line. Error bars, corresponding to one standard deviation, are shown for each fitted temperature. When saturation is not included (squares), the model predicts only low intensity regime temperatures well; the high-intensity regime temperatures deviate far above the actual temperature. When the model is based on the saturation of the B←X transition, the temperatures are too low. When both saturation of the B←X transition and the presence of the A state reactive path are included, the fitted temperatures reflect the actual temperature (<10% error) in the high-intensity regime.

On the basis of the modified rotational anisotropy equation (eq 4) and the parameter values in Table 2, as the intensity of the field increases, both the saturation parameter (A_S) and the perpendicular state parameter ($A_\perp$) increase. We have empirically determined the relationship between these parameters and the pump laser intensity. Both follow an exponential model as shown in Figure 6. (For the $A_\perp$ trend line, the second data point was not used in the fit because of its deviation from the rest of the data.) It is reasonable to expect a simple relationship between the two parameters. Notice that the values for the saturation intensity (I_0) are similar for these two trends.

A unifying equation for modeling the rotational anisotropy can be obtained if we assume that the ratio of the probabilities for probing the two pathways (β←A←X and f←B←X) is fixed and corresponds to $A_{A/B}$ as discussed earlier. Under this assumption, we obtain the following expression for the rotational anisotropy

$$r_{A_S,A_{A/B}}(j,t) = r_0(j,t) - A_S\{r_0(j,t) + A_{A/B}e^{-(t/\tau)2}\} \qquad (5)$$

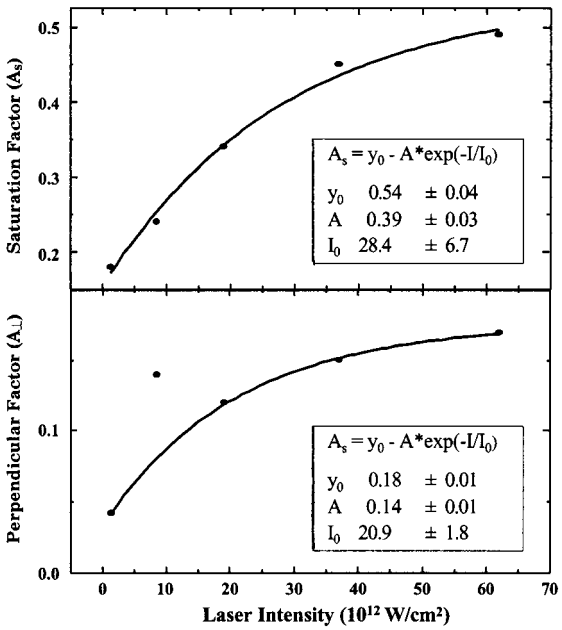

Figure 6. Dependence of the saturation (A_S) and perpendicular ($A_\perp$) parameters on the laser intensity. Both parameters show an exponential trend with similar values for the saturation intensity, I_0.

TABLE 3: Rotational Temperature Fits (T_{fit}) at Different Pump Laser Intensities Using eq 5 Which Includes the Saturation Parameter (A_S) and the Fixed $A_{A/B}$ Parameter (which is 0.49)[a]

intensity (10^{12}W/cm^2)	saturation + perpendicular parameter ($A_{A/B} = 0.490$)			
	A_S	T_{fit} (K)		% error
1.4	0.13	346	±20	16%
8.5	0.26	265	±10	(11%)
19	0.30	321	±11	8.1%
37	0.38	302	±12	1.7%
62	0.43	290	±16	(2.4%)

[a] Parentheses around a percentage indicate that the calculated temperature is below the actual temperature.

where the saturation reduces the observed B−X anisotropy and, at the same time, increases the ability to see the A−X transition. Using eq 5 in place of eq 3 (or eq 4) in the fitting procedure described above, we have fit the data by varying A_S, T_{fit}, and the background and keeping the value of $A_{A/B}$ equal to 0.49. We have found satisfactory agreement between T_{fit} and T_{RT} with 1.7−16% deviation (see Table 3).

V. Conclusions

Ultrafast rotational anisotropy measurements are important for determining the rotational characteristics of nonreactive and reactive systems. Therefore, being able to reliably obtain quantitative rotational temperatures or rotational population distributions from experimental data is essential. As the availability of femtosecond laser systems with very high peak intensities continues to increase, it is important to understand how strong fields affect some of these measurements. Here, we explore the effect of high pump laser intensities for rotational anisotropy measurements and give a formulation that includes the loss of anisotropy caused by saturation as well as an additional parameter that, in the case of I_2, corresponds to a reactive pathway.

We have shown here how saturation effects and competing reactive pathways can be taken into account in order to fit rotational anisotropy data spanning 3 orders of magnitude in laser intensities and obtain accurate quantitative measurements. This modified rotational anisotropy model can be adapted to other systems, including reactive systems, to obtain quantitative rotational distributions and temperatures when using intense laser fields. Our results highlight the importance of repulsive potential energy surfaces in the response of molecules under strong field excitation.

Acknowledgment. Funding for this project comes from Grant No. CHE-9812584 of the National Science Foundation. M.D. is a Lucille and David Packard Science and Engineering Fellow and an Alfred P. Sloan Research Fellow. Additional funding is from a Camille Dreyfus Teacher-Scholar Award. E.J.B. is supported by a National Science Foundation Graduate Fellowship.

References and Notes

(1) *Femtochemistry*; Zewail, A. H., Ed.; World Scientific: Singapore, 1994; Vol. I and II.
(2) *Femtosecond Chemistry*; Manz, J., Woste, L., Eds.; Verlag Chemie GmbH: Weinheim, 1995; Vol. I and II.
(3) *Femtochemistry: Ultrafast Chemical and Physical Processes in Molecular Systems*; Chergui, M., Ed.; World Scientific: Singapore, 1996.
(4) Baskin, J. S.; Zewail, A. H. *J. Phys. Chem.* **1994**, *98*, 3337 and references therein.
(5) Zhang, Q.; Marvet, U.; Dantus, M. *Faraday Discussion* **1997**, *108*, 63.
(6) Zhang, Q.; Marvet, U.; Dantus, M. *J. Chem. Phys.* **1998**, *109*, 4428.
(7) Marvet, U.; Zhang, Q.; Dantus, M. *J. Phys. Chem. Special Edition*: *Femtochemistry* **1998**, *102*, 4111.
(8) Felker, P. M.; Baskin, J. S.; Zewail, A. H. *J. Phys. Chem.* **1986**, *90*, 724.
(9) Felker, P. M.; Zewail, A. H. *J. Chem. Phys.* **1987**, *86*, 2460.
(10) Dantus, M.; Bowman, R. M.; Baskin, J. S.; Zewail, A. H. *Chem. Phys. Lett.* **1989**, *159*, 406.
(11) Brown, E. J.; Zhang, Q.; Dantus, M. *J. Chem. Phys.* **1999**, *110*, 5772.
(12) Brown, E. J.; Pastirk, I.; Dantus, M. *J. Phys. Chem. A* **1999**, *103*, 2912.
(13) Dantus, M. *Annu. Rev. Phys. Chem.* **2001**, *52*, 639.
(14) Lozovoy, V. V.; Pastirk, I.; Comstock, M.; Dantus, M. *Chem. Phys.* **2001**, *266*, 205.
(15) Gordon, R. G. *J. Chem. Phys.* **1966**, *45*, 1643.
(16) Friedrich, B.; Herschbach, D. *Phys. Rev. Lett.* **1995**, *74*, 4623.
(17) Friedrich, B.; Herschbach, D. *J. Phys. Chem.* **1995**, *99*, 15686.
(18) Normand, D.; Lompré, L. A.; Cornaggia, C. *J. Phys. B* **1992**, *25*, L497.
(19) Dietrich, P.; Strickland, D. T.; Laberge, M.; Corkum, P. B. *Phys. Rev. A* **1993**, *47*, 2305.
(20) Kim, W.; Felker, P. M. *J. Chem. Phys.* **1996**, *104*, 1147.
(21) Kim, W. S.; Felker, P. M. *J. Chem. Phys.* **1997**, *107*, 2193.
(22) Sakai, H.; Safvan, C. P.; Larsen, J. J.; Hilligsøe, K. M.; Hald, K.; Stapelfeldt, H. *J. Chem. Phys.* **1999**, *110*, 10 235.
(23) Larsen, J. J.; Wendt-Larsen, I.; Stapelfeldt, H. *Phys. Rev. Lett.* **1999**, *83*, 1123.
(24) Posthumus, J. H.; Plumridge, J.; Thomas, M. K.; Codling, K.; Frasinski, L. J.; Langley, A. J.; Taday, P. F. *J. Phys. B−At. Mol. Opt. Phys.* **1998**, *31*, L553.
(25) Villeneuve, D. M.; Aseyev, S. A.; Dietrich, P.; Spanner, M.; Ivanov, M. Y.; Corkum, P. B. *Phys. Rev. Lett.* **2000**, *85*, 542.
(26) Kono, H.; Koseki, S.; Shiota, M.; Fujimura, Y. *J. Phys. Chem.* **2001**, (submitted).
(27) Comstock, M.; Pastirk, I.; Dantus, M. In *Ultrafast Phenomena XII*; Elsaesser, T., Mukamel, S., Murnane, M. M., Scherer, N. F., Eds.; 2000; p 17.
(28) Seideman, T. *J. Chem. Phys.* **1995**, *103*, 7887.
(29) Ortigoso, J.; Rodríguez, M.; Gupta, M.; Friedrich, B. *J. Chem. Phys.* **1999**, *110*, 3870.
(30) Bowman, R. M.; Dantus, M.; Zewail, A. H. *Chem. Phys. Lett.* **1989**, *161*, 297.
(31) Gruebele, M.; Roberts, G.; Dantus, M.; Bowman, R. M.; Zewail, A. H. *Chem. Phys. Lett.* **1990**, *166*, 459.
(32) Dantus, M.; Bowman, R. M.; Zewail, A. H. *Nature* **1990**, *343*, 737.
(33) Fischer, I.; Vrakking, M. J. J.; Villeneuve, D. M.; Stolow, A. *Chem. Phys.* **1996**, *207*, 331.

(34) Sarkisov, O. M.; Gostev, F. E.; Lozovoy, V. V.; Sviridenkov, E. A.; Titov, A. A.; Tovbin, D. G.; Umanskii, S. Y. *Russ. Chem. Bull.* **1996**, *45*, 553.

(35) Lozovoy, V. V.; Antipin, S. A.; Gostev, F. E.; Titov, A. A.; Tovbin, D. G.; Sarkisov, O. M.; Vetchinkin, A. S.; Umanskii, S. Y. *Chem. Phys. Lett.* **1998**, *284*, 221.

(36) Yakovlev, V. V.; Bardeen, C. J.; Che, J. W.; Cao, J. S.; Wilson, K. R. *J. Chem. Phys.* **1998**, *108*, 2309.

(37) Lozovoy, V. V.; Pastirk, I.; Brown, E. J.; Grimberg, B. I.; Dantus, M. *Intl. Rev. Phys. Chem.* **2000**, *19*, 531.

(38) LeRoy, R. J. *J. Chem. Phys.* **1970**, *52*, 2683.

(39) Steinfeld, J. I.; Zare, R. N.; Jones, L.; Lesk, M.; Klemperer, W. *J. Chem. Phys.* **1965**, *42*, 25.

(40) Brand, J. C. D.; Hoy, A. R. *Can. J. Phys.* **1982**, *60*, 1209.

(41) Brand, J. C. D.; Hoy, A. R.; Kalkar, A. K.; Yamashita, A. B. *J. Mol. Spectrosc.* **1982**, *95*, 350.

(42) Heemann, U.; Knöckel, H.; Tiemann, E. *Chem. Phys. Lett.* **1982**, *90*, 17.

(43) Holmes, A. J.; Lawley, K. P.; Ridley, T.; Donovan, R. J.; Langridge-Smith, P. R. R. *J. Chem. Soc., Faraday Trans.* **1991**, *87*, 15.

(44) Zare, R. N. *Mol. Photochem.* **1972**, *4*, 1.

(45) Marvet, U.; Zhang, Q.; Brown, E. J.; Dantus, M. *J. Chem. Phys.* **1998**, *109*, 4415.

(46) Tellinghuisen, J. *J. Chem. Phys.* **1973**, *58*, 2821.

(47) Tellinghuisen, J. *J. Chem. Phys.* **1982**, *76*, 4736.

(48) Perrot, J. P.; Femelat, B.; Subtil, J. L.; Broyer, M.; Chevaleyre, J. *Mol. Phys.* **1987**, *61*, 85.

(49) Zheng, X.; Fei, S.; Heaven, M. C.; Tellinghuisen, J. *J. Mol. Spectrosc.* **1991**, *149*, 399.

(50) Lawley, K.; Jewsbury, P.; Ridley, T.; Langridge-Smith, P.; Donovan, R. *Mol. Phys.* **1992**, *75*, 811.

(51) Liu, Q. L.; Wang, J.-K.; Zewail, A. H. *Nature* **1993**, *364*, 427.

(52) Wang, J.-K.; Liu, Q. L.; Zewail, A. H. *J. Phys. Chem.* **1995**, *99*, 11 309.